PLOS ONE

RESEARCH ARTICLE

Molecular basis of the reaction mechanism of the methyltransferase HENMT1

Philipp Kaldis[1,2], **Li Na Zhao**[1]*

1 Department of Clinical Sciences, Lund University, Malmö, Skåne, Sweden, 2 Lund University Diabetes Centre, Lund University, Malmö, Skåne, Sweden

* lina.zhao@med.lu.se

Citation: Kaldis P, Zhao LN (2024) Molecular basis of the reaction mechanism of the methyltransferase HENMT1. PLoS ONE 19(1): e0293243. https://doi.org/10.1371/journal.pone.0293243

Editor: Kshatresh Dutta Dubey, Shiv Nadar University, INDIA

Received: June 12, 2023

Accepted: October 9, 2023

Published: January 10, 2024

Data Availability Statement: All relevant data are within the paper and its Supporting Information files.

Funding: This work is supported by IngaBritt och Arne Lundbergs Forskningsstiftelse [LU2020-0013], the Crafoord Foundation [Ref. No. 20210516, Ref. No. 20220582], and Åke Wibergs Stiftelse [Ref. No. M21-0048] to L.N.Z. P.K is supported by the Swedish Research Council [2021-01331], the Swedish Cancer Society [Cancerfonden 21-1566Pj], Crafoord Foundation [Ref. No. 20220628], the Faculty of Medicine, Lund

Abstract

PIWI-interacting RNAs (piRNAs) are important for ensuring the integrity of the germline. 3'-terminal 2'-O-methylation is essential for piRNA maturation and to protect them from degradation. HENMT1 (HEN Methyltransferase 1) carries out the 2'-O-methylation, which is of key importance for piRNA stability and functionality. However, neither the structure nor the catalytic mechanism of mammalian HENMT1 have been studied. We have constructed a catalytic-competent HENMT1 complex using computational approaches, in which Mg^{2+} is primarily coordinated by four evolutionary conserved residues, and is further auxiliary coordinated by the 3'-O and 2'-O on the 3'-terminal nucleotide of the piRNA. Our study suggests that metal has limited effects on substrate and cofactor binding but is essential for catalysis. The reaction consists of deprotonation of the 2'-OH to 2'-O and a methyl transfer from SAM to the 2'-O. The methyl transfer is spontaneous and fast. Our in-depth analysis suggests that the 2'-OH may be deprotonated before entering the active site or it may be partially deprotonated at the active site by His800 and Asp859, which are in a special alignment that facilitates the proton transfer out of the active site. Furthermore, we have developed a detailed potential reaction scenario indicating that HENMT1 is Mg^{2+} utilizing but is not a Mg^{2+} dependent enzyme.

Introduction

RNA modification proteins (RMPs) are (i) enzymes that covalently modify RNA molecules ("writers"); (ii) enzymes that reverse these modifications ("erasers"); and (iii) proteins that recognize and selectively bind these modified RNAs ("readers") [1, 2]. RMPs play a myriad of roles in the structural integrity and translational fidelity of RNAs. The mechanisms of adding, removing, and recognizing a chemical group in RNAs has been referred to as epitranscriptomics. Emerging data has suggested that epitranscriptomics is an important indicator in cancer and other diseases, and RMPs have emerged as a new class of therapeutic targets with a burst of research interest in recent years [1, 3].

Over 100 types of reversible and dynamic chemical modifications are carried out by RMPs on cellular RNAs [4, 5]. In cancer, 27% of all known human RMPs are dysregulated, among them HENMT1 and LAGE3 have been reported to be the two most frequently overexpressed genes across a wide variety of cancer types. They are consistently overexpressed in tumors at

University to PK, the Swedish Foundation for Strategic Research [Dnr IRC15-0067], and Swedish Research Council, Strategic Research Area EXODIAB [Dnr 2009-1039]. In addition, the computations were enabled by resources provided by the Swedish National Infrastructure for Computing (SNIC) on resource Kebnekaise at HPC2N partially funded by the Swedish Research Council through grant agreement no. 2018-05973. The funders had no role in study design, data collection and analysis, decision to publish, or preparation of the manuscript. The funders had no role in study design, data collection and analysis, decision to publish, or preparation of the manuscript.

Competing interests: The authors have declared that no competing interests exist.

Abbreviations: 2'O-me, 2' O-methylation; AGO2, Argonaute RISC Catalytic Component 2; CTD, C-terminal domain; EVB, empirical valence bond; HEN1-FL, full-length plant HEN1; HEN1-M, truncated plant HEN1; HENMT1, Hua ENhancer (HEN) methyltransferase 1; LRA, Linear Response Approximation; MCPT, Monte Carlo proton transfer; miRNAs, microRNAs; NSCLC, non-small cell lung cancer; nt, nucleotides; PDCD4, programmed cell death protein 4; PDLD/S-LRA/β, LRA version of Protein Dipoles Langevin Dipoles β version; piRNAs, P-element-induced wimpy testis-interacting RNAs; PTEN, phosphatase and tensin homolog; RECK, reversion-inducing cysteine-rich protein with Kazal motifs; RMPs, RNA modification proteins; SAH, S-Adenosyl-L-homocysteine; SAM, S-adenosylmethionine; SCAAS, surface-constraint all-atom solvent; sncRNAs, small noncoding RNAs; STAT3, signal transducer activator of transcription 3.

various stages of progression, particularly at stages III and IV, and have been suggested to be promising drug targets for anti-tumor therapies [6].

The Hua ENhancer (HEN) methyltransferase 1 (HENMT1; C1orf59; EC 2.1.1.n8; UniPort ID: Q5T8I9) has a pronounced role in 2' O-methylation (2'-Ome) of mammalian P-element-induced wimpy testis-interacting RNAs (piRNAs) which are critical in the early phases of spermatogenesis, and the repression of adult male germ cell transposons. HENMT1 loss-of-function induces piRNA instability and ultimately leads to male sterility [7, 8]. Recently, HENMT1 was shown to be responsible for the methylation of the 3'-terminal 2'-Ome of mammalian miR-21-5p (see "micro RNA" section in S1 File.pdf), which plays a predominant role in human non-small cell lung cancer (NSCLC).

piRNAs are well-defined in the male and female germline, with hundreds of thousands of unique piRNAs in mammals (27,700 sequence in piRNAdb.hsa.v1_7_6.fa from piRNAdb.org [9]; 282,235 clustered piRNAs from piRNA cluster database [10–12]; and 667,944 from piRNABank [13, 14]. The length of piRNAs varies from 21–31 nt among species with a common and predominant 5' uridine (U) and conserved A at position 10, but with a less defined secondary structure [15]. In somatic cells, piRNA dysregulation has been associated with tumor development and metastasis and has the potential to predict cancer prognosis [16, 17].

The 2'-O-methylation on the 3'-terminal of a subset of small RNAs is a crucial step for their functional maturation and is prevalent among fungi, plants, and animals, which is achieved by a conserved SAM-dependent RNA methyltransferase, HEN1 and its homologues. Structural studies of plant HEN1 with a 22 nt RNA duplex and the cofactor product SAH, revealed that Mg^{2+} is coordinated by both 2' and 3' hydroxyls on the 3'-terminal of the 22 nt RNA and four residues (Glu796, Glu799, His800, and His860; corresponding to E133, E136, H137 and H182 in mouse; and E132, E135, H136, and H181 in human) at the active site of the methyltransferase domain [18]. The SAM-binding pocket is formed by five consecutive residues $_{719}$DFGCG$_{723}$ residing adjacent to the catalytic domain of *Arabidopsis* HEN1. Furthermore, the mechanism of 2'-O-methylation has been suggested to be Mg^{2+}-dependent for plant HEN1 [18]. The substrate specificity of plant HEN1 is well-defined since it can methylate both microRNA and small interfering RNAs duplexes (miRNA/miRNA* or siRNA/siRNA*), with a preferred length of 21–24 nt, RNA duplexes with 2 nt overhang, and free 2'- and 3'-hydroxyls on the 3' terminal nucleotide [19, 20]. The MTase domain of Drosophila HEN1 is located at its *N*-terminus and biochemical assays indicate that it can methylate small single-stranded RNAs but not double-stranded RNAs [21, 22]. Four crystal structures (PDB IDs: 3JWG, 3JWI, 3JWH, and 3JWJ) of the MTase domain of a bacterial homolog of HEN1 demonstrate a unique motif and a domain that are specific for RNA recognition and catalysis [23], with the FXPP motif being important for substrate binding [24]. The mouse homolog of HEN1 (mHEN1) is expressed predominantly in testis and methylates the 3′ end of piRNAs in vitro [25]. The methylation efficiency for piRNAs with different 3' end nucleotide are: A (259%) > C (137%) > U (100%) > G (44%) [25]. mHEN1 does not recognize the 5' end of the substrate and is not particularly specific about the length of RNA substrate [25].

The architecture of human HENMT1 (393 aa) consists of a confirmed MTase domain, which alone cannot confer catalytic activity [24]. However, including the $_{27}$FKPP$_{30}$ motif at the very *N*-terminus, namely the 26–263 region (below we refer to it as MTase region), confers full activity of the MTase activity in vitro [24]. Unlike plant HEN1, which methylates double-stranded RNA, the mammalian HEN1 methylates only single-stranded RNA [24]. The *C*-terminal domain (CTD, ~263–393) of HENMT1 lacks homology in the primary sequence, which indicates that the CTD varies substantially across species. However, there is a possibility that the *C*-terminal domain may together with the very *N*-terminus, cooperatively recognize and bind the substrate; or HENMT1 interacts with other proteins to facilitate its localization as was observed for zebrafish HEN1 [26].

The MTase region of human HENMT1 crystallized with SAH (PDB ID: 4XCX) and SAM (PDB ID: 5WY0) is missing the important cofactor Mg^{2+}. Moreover, human HENMT1 has been reported to prefer Mn2+ over Mg2+, similar to bacteria HEN1 [24]. Glu132, Glu135, His136, and His181, corresponding to Glu796, Glu799, His800 and His860 in plant HEN1, were proposed to be responsible for Mg^{2+} binding by (a) manual assertion inferred from sequence alignment in UniPort entry Q5T8I9; and (b) comparison with HEN1 from plant (PDB ID: 3HTX) [27].

Despite the structural and biochemical advance in studying HENMT1, there are still many questions unanswered [24]. This includes, (a) what is the complete list of substrates of HENMT1? Are piRNAs and miR-21-5p the only substrates? and (b) what is the molecular basis of HENMT1 catalytic activity? Here, we aim to use computational biochemical approaches to investigate the mechanisms driving mammalian HENMT1 activity.

From our previous work, we have observed that (a) the energy required for the methyl transfer in SAM-dependent methyltransferases is around 8 k_{cal}/mol in protein and 13.8 k_{cal}/mol in water, which is close to the spontaneous transfer under thermodynamic conditions; and (b) the proton transfer is a rate-limiting step [28]. Transferring this knowledge to plant HEN1 and mammalian HENMT1, we will consider and examine five potential reaction mechanisms for the rate-limiting proton transfer step: (I) 2'-OH is deprotonated before it reaches the active site in the reaction-ready state; (II) a hydroxide present at the active site acts as base to withdraw the proton; (III) His800 acts as a base; (IV) Glu796 acts as a base; and (V) His800 and Asp859, in a special alignment, facilitate the proton transfer out of the active site.

By compiling available structural information of HENMT1, computational modeling, calculating free energies, as well as a detailed analysis and carefully evaluation of possible mechanisms, we have reached the conclusion that the hydrogen from the 2'-OH has the possibility to be deprotonated before entering the active site; or it is partially deprotonated once entering the active site due to its interaction with the residues (Glu796 and His800) at the active site; or the spatial alignment of Asp796 and His800 may facilitate the transport of the hydrogen out of the pocket. In addition, we propose an equilibrium ordered kinetic mechanism in which SAM and Mg^{2+} bind first prior to substrate binding.

Material and methods

Structure preparation

Since the truncated *C*-terminal domain (residues 666–942) of plant HEN1 and MTase region of HENMT1 are sufficient for the methyltransferase activity, here we used the truncated plant HEN1 methyltransferase domain (HEN1-M) and MTase region of HENMT1 for our computational analysis. We have built 3 systems: (SI) plant HEN1-M with 2'-OH binding to Mg^{2+} directly; (SII) plant HEN1-M with 2'-OH binding to Mg^{2+} through hydroxide mediated interactions, termed as HEN1-W; and (SIII) mammalian HENMT1 with 2'-OH binding to Mg^{2+} through hydroxide mediated interactions. 3HTX.pdb was the primary template used for the analysis of HEN1-W and HEN1-M. SAH was converted back to SAM by adding a methyl group using Avogadro (S1 Fig). The missing loops ($_{839}$TPETQEENNSEP$_{850}$ and $_{912}$SVENV$_{916}$) were built and refined using LoopModel and DOPE LoopModel modules within MODELLER10 [29] while the top 10 out of 400 models were optimized and relaxed within MOLARIX-XG.

For human HENMT1, the canonical sequence 26–263, featuring the MTase domain, was taken from uniprot (ID Q5T8I9). The crystal structure of the human MTase region of HENMT1 in complex with SAH (PDB ID: 4XCX; covering sequence 26–170, 180–232, and 244–262) and SAM (PDB ID: 5WY0; covering sequence 31–85, 105–173, 177–236, and 245–

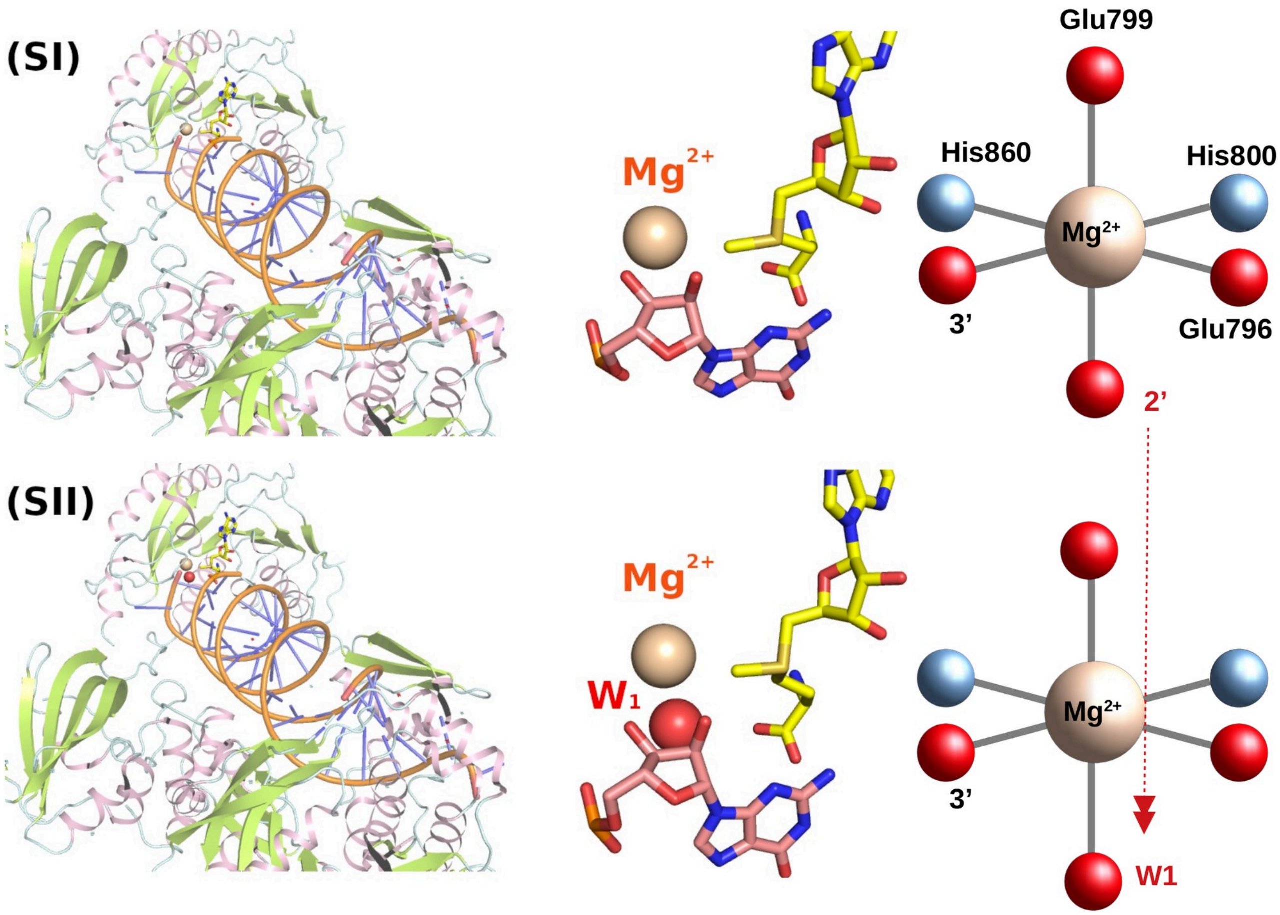

Fig 1. Plant HEN1 with 2'-O and 3'-O groups directly coordinating Mg^{2+} (SI). Plant HEN1 with hydroxide and 3'-O groups coordinating Mg^{2+} (SII).

https://doi.org/10.1371/journal.pone.0293243.g001

258) were used as templates for modeling the MTase region of the HENMT1 complex with cofactor SAM [Fig 1(A)]. The automodel and loopmodel modules within MODELLER 10 were used to build 200 models and loop refinement. The final models were selected based on the objective function; the four residues (Glu132, Glu135, His136, and His181) that directly bind Mg^{2+} were refined based on plant HEN1 (3HTX.pdb). Note that the crystal water (W1) from 5WY0.pdb was kept for SII and SIII. The structures were further optimized and relaxed by MD simulations within the MOLARIX-XG package before the free energy calculation.

For plant HEN1, the miR173/miR173* duplex, crystallized in 3HTX, was experimentally generated using synthesized miR173 and miR173* RNA oligonucleotides with 5′ P and 3′ OH annealed [19]. Note that the 2nt 3′ overhang is an important feature of the substrate. The configuration for the miR173/miR173*(22A), miR173/miR173*(22C), miR173/miR173*(22U) are generated by directly mutating the 22nd nucleotide. For plant HEN1, the configurations with the lowest binding energy towards the substrate were selected and used for the subsequent reaction calculation.

Binding energy calculations

Binding energy calculations were carried out to examine (a) the truncated HEN1 (HEN1-M), and (b) to determine the role of the Mg^{2+}. We calculated the binding energy of SAM and substrate, which is a small RNA duplex, derived from one natural substrates of plant HEN1, termed miR173/miR173* [18], in the presence/absence of Mg^{2+} using the Linear Response Approximation (LRA) version of Protein Dipoles Langevin Dipoles (PDLD/S-LRA) method and also its PDLD/S-LRA/β version [30] within MOLARIS-XG package. At first, we generated both complexes with full length HEN1 (HEN1-FL) and truncated HEN1 featuring the methyltransferase domain (HEN1-M) with and without Mg^{2+} configurations, and with the charged and uncharged forms of solute, respectively, and then treated the long-range interaction with the local reaction field (LRF) [31]. After explicit all-atom molecular dynamics simulations of all above complexes, each lasting 2ps, with the surface-constrained all-atom solvent (SCAAS) [32], we carried out the PDLD/S calculations on the generated configurations. We took the average value as the consistent estimation of the binding free energy. A 2ps run was done for each of these simulations at 300K. The philosophy behind this method has been discussed in Ref. [30] and in our previous work [28].

Simulations

The 2'-O-methylation requires two steps: deprotonation of the 2'-OH group preceding the transfer of the methyl group from SAM to 2'-O group. First, we started from the methyl transfer from SAM to 2'-O and later addressed the deprotonation of the 2'-OH group. The initial kinetic descriptions were done at the M06-2X/6-31++G(d,p) level which provide a fine balance between the computational costs and the reliability of results with a continuum solvent model. Mg^{2+} and the surrounding ligands (2'-O/H_2O/OH^-, 3'-O, Glu796, Glu799, His800 and His860) were included in the QM region (consisting of 83 atoms). The results from the DFT calculation are then used to calibrate empirical valence bond (EVB) parameters for the methyl transfer in enzymes, both plant HEN1 and HENMT1. The active site region was immersed in a 32Å sphere of water molecules using the surface-constraint all-atom solvent (SCAAS) type boundary condition [32]. The geometric center of the EVB reacting atoms was set as the center of the simulation sphere. The Langevin dipoles was applied outside of this 32Å region, followed by a bulk continuum. The long-range electrostatics were treated with the local reaction field (LRF) method. Atoms beyond the sphere were fixed at their initial positions and no electrostatic interaction from outside of the sphere was considered. In order to determine the protonation state and optimize the charge distribution of all ionizable residues, we were using the Monte Carlo proton transfer (MCPT) algorithm which simulates the proton transfer between charged residues. The charge distribution was updated and evaluated with Monte Carlo approaches to identify the optimal charge distribution. The protonation state of the ionizable residues are shown in S2 Fig. The detailed EVB simulation procedures are described in our previous work [28, 33, 34]. The EVB simulations of the methyl transfer were done using the Enzymix module within the MOLARIS-XG package [32, 35]. Note that all the DFT calculations were done using Gaussian 16 Revision C.01 [36].

Results

Overview of modeled HENMT1 structure

The overview of modeled HENMT1 is shown in Fig 2A. After detailed structural analysis, we believe that Glu132, Glu135, His136, and His181 constitute the predominant motif involved in binding Mg^{2+} which can then attract 3'-terminal miRNAs or piRNAs by forming a hydrogen bond with the 3'-OH group of the ribose moiety (Fig 2B). In addition, the 2'- and 3'-hydroxyl groups of piRNA bind Mg^{2+} directly in the presence of SAH (Fig 2B).

The plant HEN1 protein not merely has a putative dsRNA binding motif at the *N*-terminus, but also has a conserved SAM-binding motif in the *C*-terminal region [2, 19]. Here, we have

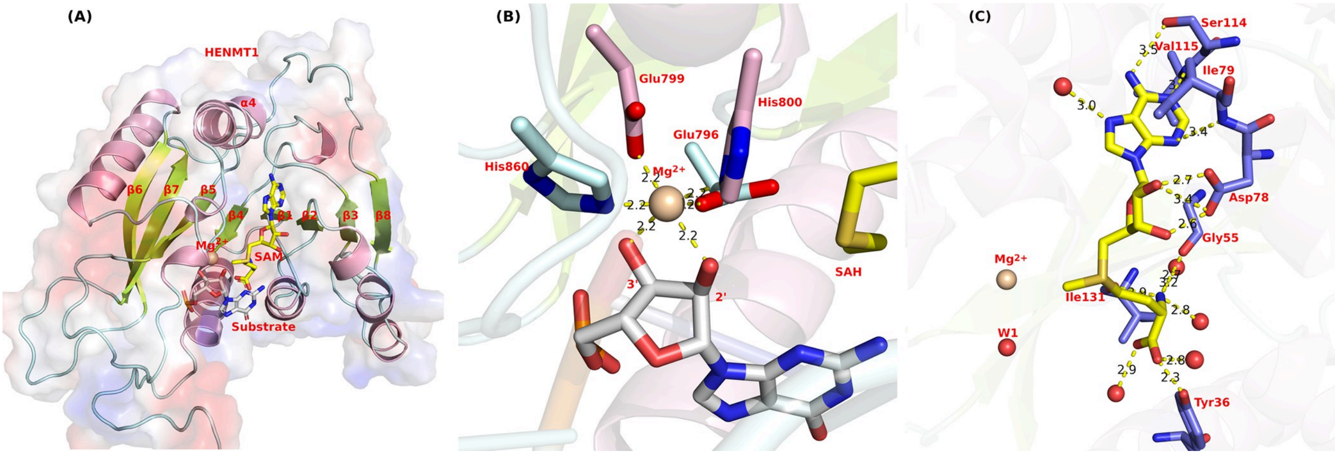

Fig 2. (A) Overview of modeled HENMT1 structure. (B) The Mg^{2+} binding pocket from plant HEN1 (PDB ID: 3HTX). Helices are colored as pink for the C atoms, palecyan for the residues from the loop, and lemon color for the C atoms from β-sheet. (C) The SAM binding pocket (PDB ID: 5WY0) with Mg^{2+} superimposed from 3HTX. The water molecule (W1) is crystal water from 5WY0.pdb.

https://doi.org/10.1371/journal.pone.0293243.g002

systematically examined this SAM binding pocket. There are two peptide motifs conserved among plant, mouse, and human isoforms of the canonical SAM binding site; namely, $_{717}$LVDFGCG$_{723}$ and $_{743}$GVDI$_{746}$ in plant HEN1; $_{52}$VADLGCG$_{58}$ and $_{77}$GVDI$_{80}$ in mouse HEN1; and $_{51}$VADLGCG$_{57}$ and $_{76}$GVDI$_{79}$ in human HENMT1.

Fig 2C depicts the interaction scenario of SAM with HENMT1 in detail. The adenine base of SAM is coordinated by the side chain of Ser114, the backbone of Val115 and Ile79, and a water molecule. The ribose group of SAM is coordinated by equivalent bidentate hydrogen bond interactions between its hydroxyl and the carboxyl group of Asp78. The amino group of methionine is forming a hydrogen bond with the backbone of Gly55 and Ile131, and two water molecules; while the carboxyl group of methionine is forming a hydrogen bond with side chain of Tyr36 and two water molecules. Taken together, we have identified residues 55, 78, 79 from conserved motifs that are directly binding SAM, and are conserved among plant HEN1, mouse HEN1, and HENMT1.

2'-OH deprotonation

The 2-O methylation requires two steps: (a) the deprotonation of the 2-OH group, and (b) the transfer of a methyl group from SAM to the deprotonated 2-O group. The deprotonation is the prerequisite and it is usually elusive. Since these steps hard to determine with theoretical or empirical methods due to the short time frame, we are trying various different mechanisms to determine which one is the most likely.

We have considered five potential mechanisms (Fig 3): Mechanism I is based on deprotonation during the process when substrate is recruited at the active site. Our calculations, however, determined that the 2'-OH of the ribose sugar has a high instinct p*K*a (12~14), which is usually neutral at biological pH [37]. Hence, we have considered the possibility that 2'-O(H) still has the H once it enters the reactive site, which needs a base to remove this H. Mechanism II is based on a hydroxide/water present at the active site of HENMT1 crystal structure (5WY0) to deprotonate the 2'-OH. Mechanism III is based on His800 deprotonating the 2'-OH group. Nevertheless, scrutinizing the crystal structure of plant HEN1 (3HTX), we found that the pKa of His800 (corresponds to His136 in HENMT1) is calculated to be 10.2, which indicated that it binds proton tightly, increasing the likeliness that the hydrogens are on both the δ and ε sites

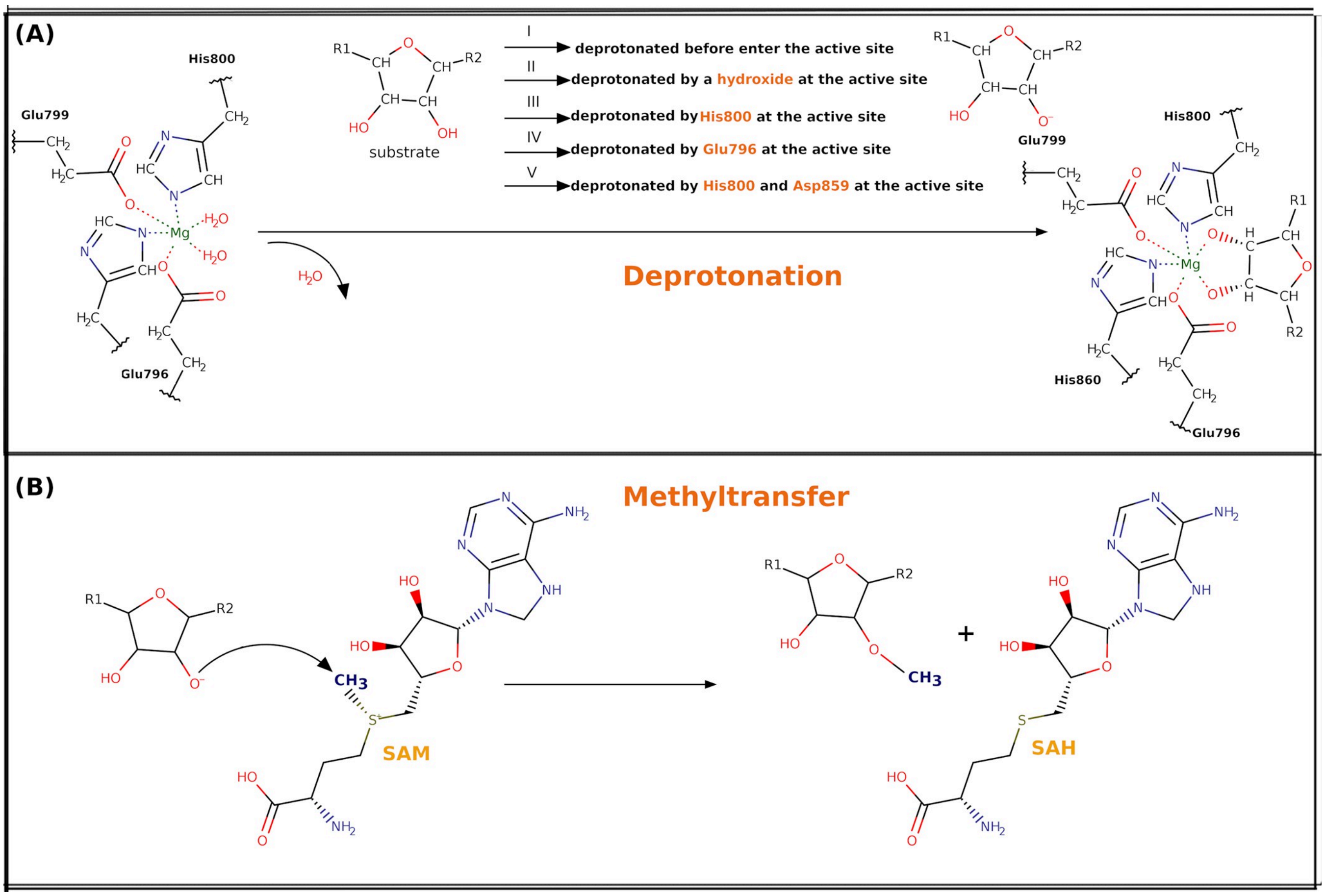

Fig 3. The reaction scheme of the deprotonation and methyltransfer.

https://doi.org/10.1371/journal.pone.0293243.g003

at product state, supporting a mechanism, in which His800 deprotonates the 2'-OH. Mechanism IV is based on Glu796 deprotonating the 2'-OH group. This is however unlikely due to the unusually low pKa value of Glu796 which is estimated to be 1.02 and Glu796 is in the immediate vicinity of 2'-OH. Mechanism V is based on structural observations concerning the spatial alignment of His800 and Asp859, as well as surrounding residues facilitating a proton transfer network to deliver the proton out of the active site. Specifically, Asp859 abstracts a hydrogen from His800 at the δ site and His800 withdraws the hydrogen from the 2'-OH group to its ε site.

There are several possibilities for the mechanism that the hydrogen on the 2'-OH group may be lost or still bonds in the process of substrate recruitment to the active site. One possibility is that the 2'-OH group was deprotonated during its recruitment into the active site. Once at the active site, 2'-OH may be (a) already deprotonated; (b) partial deprotonated; or (c) still protonated. For the possibility that 2'-OH needs to be deprotonated at the active site, we started to examine the potential orientation of this hydrogen because this determines the potential base that will extract this hydrogen. One approach is to infer from the potential occurrence of hydrogen bonds based on the positions of proximity heavy atoms from the X-ray structures. This inference of precise orientation of the 2'-O-H bond is of great importance in clarifying the elusive step of the 2'-OH deprotonation by revealing to which heavy atom the proton will be transferred to.

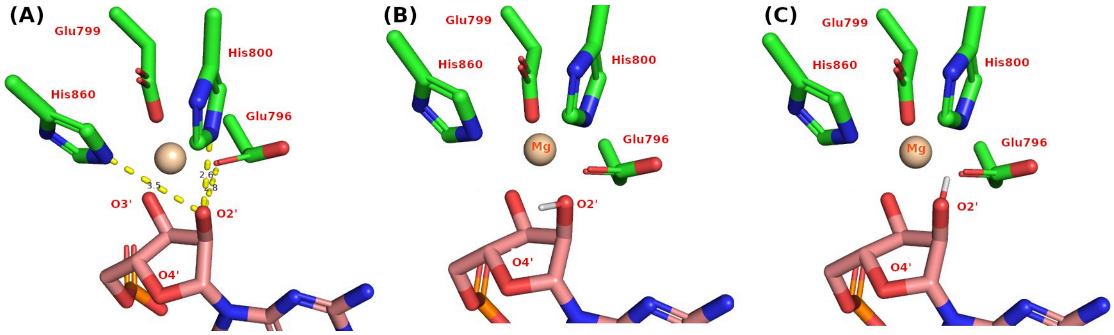

Fig 4. The potential hydrogen bonds and hydrogen orientations. (A) The potential hydrogen bond between the 2'-OH group and the surrounding atoms. (B) Hydrogen orientates towards the O4' of the same sugar related to the hydrogen bond with His860. (C) Hydrogen away from the O4' of the same sugar, related to the hydrogen bond forming with His800 and Glu796.

https://doi.org/10.1371/journal.pone.0293243.g004

There are two possible orientations of hydrogen of the 2'-hydroxyl group based on the hydrogen bond geometry criteria. The possible hydrogen bonds are illustrated in Fig 4A, and the possible orientation of the hydrogen either towards (i) O4' of the same sugar [Fig 4B], or (ii) away from the O4' of the same sugar [Fig 4C].

When hydrogen is orientated towards the direction of Glu796 and His800, our QM calculation of the active site indicate that O2' is partially deprotonated (S5 Fig), while Glu796 and 2'-O share the hydrogen with $d_{O2'\text{-}H}$ = 1.02Å and $d_{Glu796\text{-}O}$ = 1.58Å. Because of this, the orientation of the hydrogen at O2' is essential to know.

Presence of water/hydroxide at the active site. In order to understand the chemical reactions, we have calculated the pKa value of the residues at the active site using both PropKa and MCPT approaches. The pKa value of residues His800, His860, Glu796, and Glu799 were calculated based on the plant HEN1 crystal structure (3HTX.pdb) using PropKa [38] and are 10.2, 5.3, 1.0, and 7.7, respectively. Note that the crystal structure 3HTX was obtained at pH 4.8. Based on the pKa calculation, we conclude that His800 is a strong base and strongly bound to the positively charged Mg^{2+}. Glu796 and Glu799 are negatively charged; the lower pKa value of Glu796 may also be due to its binding to Mg^{2+}. A more thorough calculation using MCPT confirms the pKa value calculated by PropKa. Since 3HTX is obtained with the pronounced product SAH, we postulate that His800 and Glu796 are at the product state, which implies a possible mechanism with His800 is withdrawing a proton. Even though His800 may help deprotonate the 2'-OH for the subsequent methyl transfer, it will not be energy favorable to replace the hydrogen and Mg^{2+} that tightly binds the N_{δ} and N_{ε} with the hydrogen from 2'-OH.

Since Mg^{2+} is positively charged, it would be electrostatically favorable to bring the substrate with 2'-O rather 2'-OH in close proximity towards Mg^{2+}. If 2'-OH is deprotonated *in situ*, an external base must be coordinated by Mg^{2+}. Since Mg^{2+} already has four firm coordination atoms, together with the incoming 2'-O(H) and 3'-OH group from the substrate, resulting in a perfect six coordination as preferred by Mg^{2+}, indicating a lack of right coordination for an external base. Therefore, such an external base may be present during the process when the substrate was recruited to the active site. The external base (with a high likelihood to be a hydroxide) may abstract a proton from 2'-OH, which is quite likely because a heavy O atom was crystallized near the active site before the substrate was recruited in the HENMT1 complex with SAM (5WY0.pdb). We have excluded that the heavy O atom is water because the energy barrier of deprotonation of water is estimated to be 29 k_{cal}/mol [39], rendering it not energy feasible. A previous study has shown that the energy cost to transfer a hydroxide from the bulk solution to the Mg^{2+} coordination shell is about 5 k_{cal}/mol [39], and the free energy of hydroxide ion formation based on $k_B Tln(10)(15.7 - 7.4)$ is 11.3 k_{cal}/mol at pH 7.4. Therefore, the hypothesis that a hydroxide is present is more likely than a water for the reaction to take place.

The catalytic cycle of HENMT1 starts with hydrated metal [termed as M; $Mg^{2+}(H_20)_6$ or $Mn^{2+}(H_20)_6$] binding to HENMT1 forming a binary complex (E·M) with the replacement of 4 water molecules. SAM binding to HENMT1 has no direct contact with metal. During RNA substrate binding, it is possible that the 3'-O of the ribose moiety from the substrate would replace one O from the inner sphere of Mg^{2+}/Mn^{2+}, however, it is not energetically favorable to have the 2'-OH group of the substrate to replace the last O atom at the inner sphere of Mg^{2+}. The reason is that (a) the remaining O provides a base to abstract the proton from 2'-OH for the proceeding methyl transfer since no other base is available in the immediate vicinity; and (b) it is electrostatically favorable for a positively charged methyl group (-CH_3) to transfer to 2'-O that is directly coordinated by water rather than the positively charged Mg^{2+}. If the 2'-OH binds Mg^{2+} directly, it is not electrostatic favorable for the methyl group (-CH_3^+) to come to the 2'-O group which has +2 charge in the immediate vicinity. In addition, a base is required to deprotonate the 2'-OH for the forthcoming methyl transfer, and the only two potential base residues (Glu796 and His800 in HEN1; Glu132 and His136 in HENMT1) at the active site are directly bound to the Mg^{2+} (equal to 2 protons) which is not electrostatic favorable to withdraw another proton from 2'-OH group. Recently a water/hydroxide (W1 in Fig 2C) in the active site of human HENMT1 was reported [24]. Therefore, we first assumed that (a) W1 instead of 2'-OH provides the direct binding to Mg^{2+} and (b) W1 as hydroxide withdraws the proton from 2'-OH, which also solves the piece of the puzzle lacking a base to deprotonate the 2'-OH group. However, W1 exists in the active site which is lacking metal and substrate (5WY0.pdb). It is highly likely once the metal and substrate binding happened, the water will not be there anymore, which is evident in 3HTX.pdb. Meanwhile, we have tried the water flooding approach (S1 File) in an attempt to saturate the active site with water and found it is not possible to insert water. Furthermore, we were unable to identify the transition state for this speculated proton transfer to happen. Therefore, we have excluded the possibility of a hydride/water at the active site acting as a base to facilitate the 2-OH deprotonation. Cumulatively, our above structural analysis provides a foundation for our catalytic mechanism study.

The role of Mg^{2+}

Mg^{2+} possesses a strict octahedral geometry with a coordination number 6. Initial scrutinizing the crystal structure of plant HEN1 (PDB ID: 3HTX), we find that Glu796, Glu799, His800, and His860 together with the 2'- and 3'-OH of the substrate RNA, fulfill the coordination requirement of Mg^{2+}, and Mg^{2+} plays a direct structural role at active site. However, this structure does not reflect the reaction scenario since it is a chimera of product and reactant: (a) the product SAH is in the pocket instead of the reactant SAM; and (b) the reactant substrate is in the pocket but lacks a base to abstract the proton from the 2'-OH for the subsequent 2'-O methylation. Even though it is not a catalytic competent conformation, 3HTX provides a hallmark structure for studying HEN1.

In order to examine the role of magnesium binding, we constructed a system without Mg^{2+}, in which the protonation state of residues (Glu796, Glu799, His800, and His860) that previous coordinated the Mg^{2+} are re-evaluated and obtained similar results as the presence of Mg^{2+} (see S1 Table). Furthermore, the protonation state of His800 and His860 are both reasonably assigned on the δ site to facilitate Mg^{2+} binding.

The role of Mg^{2+} in terms of binding was calculated using the Linear Response Approximation (LRA) version of Protein Dipoles Langevin Dipoles β version (PDLD/S-LRA/β)[35] within

Table 1. The averaged absolute binding energy calculation for SAM and RNA with (w/) and without (w/o) Mg^{2+} for plant HEN1. Note that the unit is k_{cal}/mol.

Systems			Binding energy
SAM	w/ RNA	w/ Mg^{2+}	39.51
		w/o Mg^{2+}	25.39
	w/o RNA	w/ Mg^{2+}	34.19
		w/o Mg^{2+}	13.81
RNA	w/ SAM	w/ Mg^{2+}	-22.31
		w/o Mg^{2+}	-23.76
	w/o SAM	w/ Mg^{2+}	-25.82
		w/o Mg^{2+}	-23.11

https://doi.org/10.1371/journal.pone.0293243.t001

the MOLARIS-XG package. The averaged binding energy is shown in Table 1. Mg^{2+} does not enhance the positively charged cofactor SAM binding, on the contrary, it is not favorable for SAM binding. For the negatively charged substrate RNA, Mg^{2+} did not significantly enhance the substrate RNA binding. From above calculations, we have excluded a positive role of Mg^{2+} in both cofactor and substrate binding.

The properties of Mg^{2+} in the inner coordination sphere feature a very tight interaction to either water or proteins. In the case of HEN1, the inner sphere coordination of Mg^{2+} was primarily bound by four residues from protein; and its interaction with the substrate would be with the 2'-OH and 3'-OH of RNA. We studied the electrostatic role of Mg^{2+} during the methyl transfer by calculating the sum of the partial charges of the atoms [shown in Fig 5A]. However, the charge of the magnesium does not change much during the methyl transfer stage [Fig 5B].

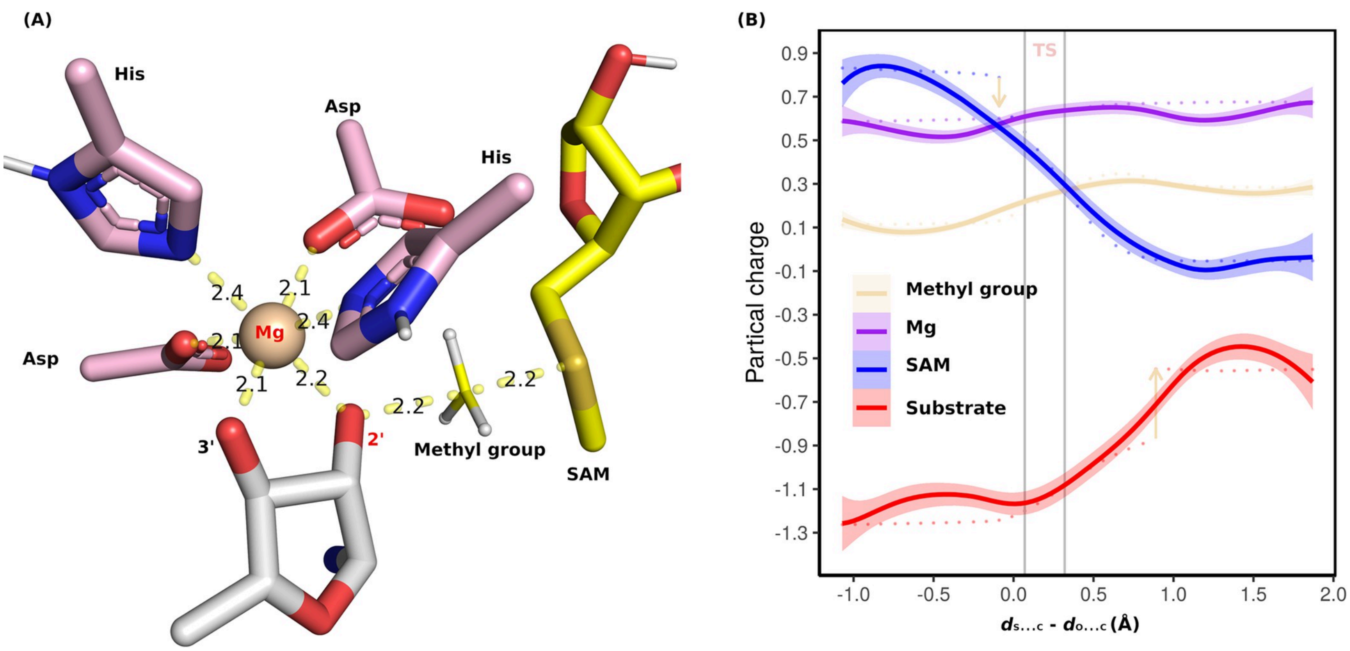

Fig 5. (A) A snapshot of the transition state (TS) for the methyl transfer. All the atoms shown above are included in our QM region. (B) Partial charge across the reaction coordinate. The x-axis indicates the distance of the reactive S from SAM and C from the methyl group minus the distance between the reactive 2'-O and the C of the methyl group. Sum of partial charges on SAM (blue), 2'-O substrate (red), methyl group (lightyellow), and Mg (purple) are indicated by lines. The down-facing arrow indicates that the charge of the methyl group starts to drift away from the SAM group, while the up-facing arrow indicates that the charge of the methyl group starts to be incorporated in the 2'-O substrate. The region between the two gray vertical bars is the TS.

https://doi.org/10.1371/journal.pone.0293243.g005

HENMT1 activity is Mg^{2+} utilizing but not Mg^{2+} dependent

First, we examined the current metal (Mg^{2+} or Mn^{2+}) binding pocket within the protein. Based on well-established knowledge about plant HEN1, we propose a couple of interaction scenarios for HENMT1 because the metal binding pocket is conserved in both plant HEN1 and human HENMT1. For HENMT1, the MTase region consists of the well-conserved seven-stranded β-sheet [40] and one extra β-sheet, in the order of 67541238, sandwiched between helices [Fig 2A]. Glu132, Glu135, and His136 are located in a short helix between β4 and α4; and His181 is located in another short helix after β5. The two short helices are two unique features in plant HEN1, which are not conserved in RNA and DNA MTases [23].

Second, we will examine the Mg^{2+} cofactor in plant HEN1 since it has been proposed that HEN1 catalytic activity is Mg^{2+} dependent [18]. Since it is well known that the distance between Mg^{2+} and its coordination oxygen atom from proteins or small molecules is around 2.07Å which was determined by crystal structures [41]. Scrutinizing the distance in the crystal structure of plant HEN1 (3HTX.pdb), we measured the distance between oxygen and metal as 2.2Å. This is outside the ideal range for Mg2+. One possible candidate metal is Mn2+. As the ionic radius of Mn^{2+} (0.75Å) is slightly bigger than Mg^{2+} (0.65Å) [41, 42], and the distance between Mn^{2+} and oxygen is 2.17Å determined by crystal structure experiments, which is 0.1Å longer than the distance between Mg^{2+} and oxygen [41, 43, 44]. The measurements of 2.2Å in plant HEN1 crystal structure are in the range of Mn^{2+}-O distance [45]. Since Mn^{2+} has the same coordination geometry as Mg^{2+}, and the experimental observation of (a) replacement of Mg^{2+} with Mn^{2+} in the Mg^{2+}-utilizing enzymes usually does not change the catalytic activity of enzymes while (b) replacing Mn^{2+} with Mg^{2+} in Mn^{2+}-dependent enzyme are less often catalytically competent [41]. Hence, we think Mn^{2+} is likely to be the alternative metal in the HEN1 binding pocket. Furthermore, the study of bacterial *Clostridium thermocellum* HEN1 (*Cth*HEN1) indicates the preference for Mn^{2+} over Mg^{2+} [46].

Third, there may be a catalytic advantage for using Mn^{2+} instead of Mg^{2+}. The optimal coordination geometries of Mg^{2+}/Mn^{2+} in proteins is octahedral, with a firm coordination number of 6. The solvent exchange rate for the inner sphere of Mg^{2+} is within 10^{-5} seconds (10^5 s^{-1}), and for Mn^{2+} is around $5 \times 10^6 s^{-1}$ [47, 48]. Mg^{2+} has a slower solvent exchange rate compared to Mn^{2+} since it has a smaller radius and higher charge density. Glu132, Glu135, His136, and His181 constitute the predominant motif in coordinating Mg^{2+}/Mn^{2+} and contribute 4 out of 6 coordination partners, while the energy penalty to reduce the coordination number from 6 is high [41]. In theory, Mg^{2+}/Mn^{2+} would interact with the 2'-OH and 3'-OH through inner sphere coordination, which implies that (a) prior to substrate binding, there maybe two water molecules that complete the 6 coordinations required by Mg^{2+}; and (b) during substrate binding, a very low rate of ligand exchange and high energy of partial dehydration may apply. As mentioned earlier, the energy penalty for loss of two waters and binding of the substrate is higher for Mg^{2+} than Mn^{2+} [41]. In terms of catalytic activity, Mn^{2+} in the binding pocket may improve the speed of the reaction.

Kinetics of plant HEN1 methyltransferase activity

Kinetic analysis of the full-length plant HEN1 (HEN1-FL) revealed that the Michaelis constants for microRNA (a synthetic RNA duplex corresponding to miR173/miR173* from *Arabidopsis thaliana*) and cofactor are $K_M^{RNA} = 0.22\mu M$ and $K_M^{SAM} = 1.7\mu M$, respectively, with an apparent catalytic turnover rate (k_{cat}) of 3.0 min^{-1} [18]. The truncated *C*-terminal domain (residues 666–942) of HEN1, termed HEN1-M, is sufficient for methylation with much higher K_M values for both RNA ($K_M^{RNA} = 2.1 \pm 0.2\mu M$) and SAM ($K_M^{SAM} > 20\mu M$), but similar k_{cat} value [49], which indicates that the *N*-terminal residues (1–665) are mainly responsible to enhance the binding of

Table 2. Calculated binding energy (k_{cal}/mol) for full-length plant HEN1 and the truncated methyltransferase domain.

System	$E^{SAM}_{binding}$	$E^{miR173}_{binding}$	$E^{miR173*}_{binding}$
HEN1-FL (w/ Mg^{2+})	39.51	-28.98	-27.37
HEN1-FL (w/o Mg^{2+})	20.55	-25.57	-23.94
HEN1-M (w/ Mg^{2+})	40.02	-26.24	-26.06
HEN1-M (w/o Mg^{2+})	20.26	-23.98	-26.97

https://doi.org/10.1371/journal.pone.0293243.t002

RNA. We have calculated the binding energy of SAM and RNA towards HEN1-FL and HEN1-M, and our results show that HEN1-FL indeed enhances the binding of RNA (see Table 2), which contributes close to 10% of the binding affinity. Further examination of the presence/absence of Mg^{2+} indicates that Mg^{2+} slightly contributes more to enhance substrate RNA binding than the *N*-terminal domain. Hence, our result confirmed that the methyltransfer domain, as a standalone catalytic domain, is the decisive factor for the methyltransferase activity.

HENMT1 substrates are not sequence-specific but there is a preference

HENMT1 contains a putative dsRNA binding motif at the *N*-terminus. We have analyzed the direct contacts of plant HEN1 and substrate. There are around 46 residues from HEN1 that have direct contacts with less than 3.5Å coordination distance (analyzed from 3HTX.pdb) from substrate. From these, 20 residues establish direct hydrogen bonding contact (S3 Fig). Scrutinizing these contacts, we found that plant HEN1 recognizes and binds substrate RNA primarily through (a) direct binding to oxygen atoms (OP1/2) of phosphate groups; and (b) O2' and O3' of the ribose hydroxyl group. There is no direct contact of plant HEN1 with nucleobases, hence, the recognition and binding are not sequence specific, which explains why plant HEN1 has a broad substrate specificity.

The architecture of HENMT1 (393 aa) consists of a confirmed MTase domain, which alone cannot confer catalytic activity, however, including the $_{27}$FKPP$_{30}$ motif at the very *N*-terminus, namely the 26–262 region (referred as MTase region), confers full activity of the MTase activity. The current available crystal structures of HENMT1 are 4XCX.pdb and 5WY0.pdb, which cover the majority of sequence from 26–262 (missing 171–179, and 233–243), and 31–258 (missing 86–104, and 237–244), respectively. There are two missing regions in the available crystal *s*tructures; 1–25 at *N*-terminus, and 263–393 at *C*-terminus. The incompleteness of the crystal structures limits our investigation regarding the substrate binding mode. Substrates of animal HEN1 and HENMT1 are predominantly small single-stranded RNAs, which can be explained by the missing dsRNA binding motif in both of them (the sequence alignment can be found in S4 Fig). This also provides a logic explanation for the findings [46] in bacterial HEN1: (a) RNA length from 12–24 nt does not affect binding but the activity decreased significantly with 9 nt RNA, and (b) substrate binding is not sequence specific except the preference for a G at the 3'-end. The knowledge gained from bacterial Hen1 regarding RNA length and RNA sequence specificity may also apply to HENMT1. However, whether the missing regions 1–25 and 31–258 contribute to the substrate recognition or binding is worthy of further study.

Discussion

The modification of piRNAs by HENMT1 plays a pivotal role since this profoundly affects the stability of piRNAs which protects the fidelity of germ line. To understand this process better, we have analyzed metal and substrate binding, as well as the kinetics of the HENMT1 methyltransfer reaction. The presence of the 2'-hydroxyl (2'-OH) group on the RNA ribose is a distinct feature that distinguishes it from DNA, which facilitates RNA structural folding and enables RNA to exert profound structural, dynamics and functional characteristics beyond the functions of DNA. However, the 2'-OH group renders RNA more vulnerable towards degradation and chemical modifications such as methylation and uridylation. For example, the 2′-OH group may nucleophilic attack its adjacent phosphate backbone, resulting in RNA self-cleavage. The 3'-terminal 2'-OH group is subjected to methylation, which in turn protects RNAs from degradation. It has been experimentally challenging to locate the precise position of the hydrogen atom of 2'-OH group or any hydrogen atoms. It is even more challenging to define whether the 2'-O group is protonated or deprotonated at the active site when the local environment involves proteins, metals and is catalytically active. For piRNA, it is crucial for the 2'-O group to be methylated for its functionality, which is carried out by HENMT1. How the 2'-OH is deprotonated and how the methyl transfer happens is largely unclear. In our work, we have attempted to understand these two processes with the precise position of hydrogen from 2'-OH holding the key to answer the elusive step of the 2'-OH deprotonation. We have carried out extensive discussions and reasoning, and our conclusion is that the hydrogen from 2'-OH is uncertain, but there are two likely possibilities for this hydrogen: (a) to be deprotonated before entering the active site or (b) successfully make it to the active site, while partially deprotonated by His800 and Asp859, which are in a special alignment that facilitates the proton transfer out of the active site. In summary, there are different possibilities for the deprotonation to happen and the environment could act as hyperparameters to "tune" the reaction.

There are few published studies of HENMT1, in fact no structure of mammalian HENMT1 with substrates has been published, and the substrates are poorly defined. In our work, we have attempted to model the HENMT1 structure inferred from plant HEN1, and we did a thorough examination of the binding pocket, in which a metal is assumed to be present and catalytically involved. Based on our detailed structural and computational studies, we believe that HENMT1 can use Mg^{2+} as cofactor, but is not Mg^{2+} dependent. It can also use Mn^{2+} as cofactor and there are advantages to using Mn^{2+} instead of Mg^{2+}.

One substantial difference between plant HEN1 and animal HEN1 is the substrate specificity. For plant HEN1, the substrates are double-stranded miRNA or siRNA duplexes, while for animal HEN1, substrates have to be single stranded. In contrast to plant HEN1, that has distinct nucleic-acid-binding channels which implies its substrate has a well-defined length (a preference for 21–24 nt RNA with a 2 nt overhangs [19, 20]) and features a distinct substrate loading and release of the cleavage product. Instead, animal HEN1, due to lack of pronounced binding grooves, has a broad substrate specificity (piRNAs, Ago2-associated siRNAs, and tRNA-derived sncRNAs) [46] with tolerance for the length of the substrate. For HENMT1, we believe that the substrate is not sequence specific, which is important for its broad substrates (different piRNA). However, HENMT1 may have preferences for substrates like small single-stranded RNAs with certain length, which will need to be studied further in the future.

Although the function of mammalian (mostly mouse) HENMT1 has been firmly established in fertility [24], there are recent reports that HENMT1 may also play an important role in some types of cancer [50]. Based on this and our own results regarding the catalytic activity of HENMT1, we assume HENMT1 plays a role in proliferation of cancer cell lines derived from many different tissues. Our analysis indicates it is associated with breast cancer, lung cancer, and skin cancer (S6 Fig). In addition, the role of HENMT1 has been characterized in male fertility, but not yet in females.

Supporting information

S1 File. Supporting information for the "molecular basis of the reaction mechanism of the methyltransferase HENMT1".
(PDF)

S1 Fig. The reconstructed model in which SAH was converted back to SAM using 3HTX as initial structure.
(TIF)

S2 Fig. Residue protonation states in the plant HEN1. Note that protonated residues are shown in red.
(TIF)

S3 Fig. The sequence alignment of HEN1 from plant, human, and mouse (uniport IDs are Q9C5Q8, Q5T8I9, and Q8CAE2). The alignment was done using Clustal Omega. This figure is generated using ESPript 3.x.
(TIF)

S4 Fig. The direct hydrogen bonding contact of plant HEN1 with its substrate miR173/miR173* based on 3HTX.pdb. The residues from plant Hen1 are shown as stick and colored yellow for C atom. The backbone of miR173/miR173* are shown as ribbon and the ribose group and base are shown as lines. This figure is generated by PyMol.
(TIF)

S5 Fig. The QM atoms used for the active site 2'-O evaluation. The white sphere is the hydrogen shared between 2'-O and Glu796.
(TIF)

S6 Fig. (A) Score distribution of HENMT1 in the genome-scale CRISPR-Cas9 screen. The x-axis represents the gene effect scores while the y axis represents the cell line distribution. Individual scores (DepMap 22Q2 Public+Score, Chronos) are indicated by the symbols depicted below the x-axis. (B) HENMT1 gene effect across different cancer types. (C) The correlation between HENMT1 gene effect (CRISPR DepMap 22Q2 Public) and its expression (Expression 22Q2 Public). The size indicates the -log10(p-value). The bigger the size corresponds to higher statistical significance. The number of points/samples are indicated in the bracket. (D) The predicted HENMT1 network, the thickness of the edge indicates the confidence score. This figure is generated using the String web server; the gene association network is predicted by STRING. (E) The correlation between HENMT1 gene effect and the expression of its associated genes based on the disease subtype and lineage subsubtype (F). (G) The expression of HENMT1 and the expression of the associated genes with statistical significance in male and female groups.
(TIF)

S1 Table. Calculated pKa for HEN1 with (w/) and without (w/o) miRNA using PropKa.
(PDF)

S2 Table. Calculated summary of the partial charge during methyl transfer.
(PDF)

S3 Table. The sequence of the small RNA duplex (derived from one natural substrate of HEN1, termed miR173/miR173*) substrate. The sequence and structure used for S1 and SII are miR173/miR173* from 3HTX.pdb. Note that the to-be-methylated strand is colored blue with the methyl 3'-end colored red.
(PDF)

Acknowledgments

L.N.Z acknowledges the computational support provided by Prof. Warshel's laboratory at the University of Southern California. L.N.Z is very grateful for the kind support from Prof. Patrik Midlöv.

Author Contributions

Conceptualization: Li Na Zhao.

Data curation: Li Na Zhao.

Formal analysis: Li Na Zhao.

Funding acquisition: Philipp Kaldis, Li Na Zhao.

Investigation: Philipp Kaldis, Li Na Zhao.

Methodology: Li Na Zhao.

Project administration: Li Na Zhao.

Resources: Li Na Zhao.

Visualization: Li Na Zhao.

Writing – original draft: Li Na Zhao.

Writing – review & editing: Philipp Kaldis, Li Na Zhao.

References

1. Boriack-Sjodin PA, Ribich S, Copeland RA. RNA-modifying proteins as anticancer drug targets. Nature Reviews Drug Discovery. 2018; 17: 435–453. https://doi.org/10.1038/nrd.2018.71 PMID: 29773918
2. Tkaczuk KL, Obarska A, Bujnicki JM. Molecular phylogenetics and comparative modeling of HEN1, a methyltransferase involved in plant microRNA biogenesis. BMC Evol Biol. 2006; 6: 6. https://doi.org/10.1186/1471-2148-6-6 PMID: 16433904
3. Shi H, Wei J, He C. Where, When, and How: Context-Dependent Functions of RNA Methylation Writers, Readers, and Erasers. Mol Cell. 2019; 74: 640–650. https://doi.org/10.1016/j.molcel.2019.04.025 PMID: 31100245
4. Roundtree IA, Evans ME, Pan T, He C. Dynamic RNA Modifications in Gene Expression Regulation. Cell. 2017; 169: 1187–1200. https://doi.org/10.1016/j.cell.2017.05.045 PMID: 28622506
5. Jonkhout N, Tran J, Smith MA, Schonrock N, Mattick JS, Novoa EM. The RNA modification landscape in human disease. RNA. 2017; 23: 1754–1769. https://doi.org/10.1261/rna.063503.117 PMID: 28855326
6. Begik O, Lucas MC, Liu H, Ramirez JM, Mattick JS, Novoa EM. Integrative analyses of the RNA modification machinery reveal tissue- and cancer-specific signatures. Genome Biol. 2020; 21: 97. https://doi.org/10.1186/s13059-020-02009-z PMID: 32375858
7. Lim SL, Qu ZP, Kortschak RD, Lawrence DM, Geoghegan J, Hempfling A-L, et al. HENMT1 and piRNA Stability Are Required for Adult Male Germ Cell Transposon Repression and to Define the Spermatogenic Program in the Mouse. PLoS Genet. 2015; 11: e1005620. https://doi.org/10.1371/journal.pgen.1005620 PMID: 26496356
8. Hempfling AL, Lim SL, Adelson DL, Evans J, O'Connor AE, Qu ZP, et al. Expression patterns of HENMT1 and PIWIL1 in human testis: implications for transposon expression. Reproduction. 2017; 154: 363–374. https://doi.org/10.1530/REP-16-0586 PMID: 28676534
9. Piuco R, Galante PAF. piRNAdb: A piwi-interacting RNA database. bioRxiv; 2021. p. 2021.09.21.461238. https://doi.org/10.1101/2021.09.21.461238
10. Gainetdinov IV, Skvortsova YV, Kondratieva SA, Klimov A, Tryakin AA, Azhikina TL. Assessment of piRNA biogenesis and function in testicular germ cell tumors and their precursor germ cell neoplasia in situ. BMC Cancer. 2018; 18: 20. https://doi.org/10.1186/s12885-017-3945-6 PMID: 29301509
11. Roovers EF, Rosenkranz D, Mahdipour M, Han C-T, He N, Chuva de Sousa Lopes SM, et al. Piwi proteins and piRNAs in mammalian oocytes and early embryos. Cell Rep. 2015; 10: 2069–2082. https://doi.org/10.1016/j.celrep.2015.02.062 PMID: 25818294
12. Williams Z, Morozov P, Mihailovic A, Lin C, Puvvula PK, Juranek S, et al. Discovery and Characterization of piRNAs in the Human Fetal Ovary. Cell Rep. 2015; 13: 854–863. https://doi.org/10.1016/j.celrep.2015.09.030 PMID: 26489470
13. Sai Lakshmi S, Agrawal S. piRNABank: a web resource on classified and clustered Piwi-interacting RNAs. Nucleic Acids Res. 2008; 36: D173–D177. https://doi.org/10.1093/nar/gkm696 PMID: 17881367

14. Das PP, Bagijn MP, Goldstein LD, Woolford JR, Lehrbach NJ, Sapetschnig A, et al. Piwi and piRNAs Act Upstream of an Endogenous siRNA Pathway to suppress Tc3 Transposon Mobility in the Caenorhabditis elegans germline. Mol Cell. 2008; 31: 79–90. https://doi.org/10.1016/j.molcel.2008.06.003 PMID: 18571451

15. Grimson A, Srivastava M, Fahey B, Woodcroft BJ, Chiang HR, King N, et al. Early origins and evolution of microRNAs and Piwi-interacting RNAs in animals. Nature. 2008; 455: 1193–1197. https://doi.org/10.1038/nature07415 PMID: 18830242

16. Jia D-D, Jiang H, Zhang Y-F, Zhang Y, Qian L-L, Zhang Y-F. The regulatory function of piRNA/PIWI complex in cancer and other human diseases: The role of DNA methylation. Int J Biol Sci. 2022; 18: 3358–3373. https://doi.org/10.7150/ijbs.68221 PMID: 35637965

17. Cheng Y, Wang Q, Jiang W, Bian Y, zhou Y, Gou A, et al. Emerging roles of piRNAs in cancer: challenges and prospects. Aging (Albany NY). 2019; 11: 9932–9946. https://doi.org/10.18632/aging.102417 PMID: 31727866

18. Huang Y, Ji L, Huang Q, Vassylyev DG, Chen X, Ma J-B. Structural insights into mechanisms of the small RNA methyltransferase HEN1. Nature. 2009; 461: 823–827. https://doi.org/10.1038/nature08433 PMID: 19812675

19. Yu B, Yang Z, Li J, Minakhina S, Yang M, Padgett RW, et al. Methylation as a Crucial Step in Plant microRNA Biogenesis. Science. 2005; 307: 932–935. https://doi.org/10.1126/science.1107130 PMID: 15705854

20. Yang Z, Ebright YW, Yu B, Chen X. HEN1 recognizes 21–24 nt small RNA duplexes and deposits a methyl group onto the 2' OH of the 3' terminal nucleotide. Nucleic Acids Res. 2006; 34: 667–675. https://doi.org/10.1093/nar/gkj474 PMID: 16449203

21. Horwich MD, Li C, Matranga C, Vagin V, Farley G, Wang P, et al. The Drosophila RNA methyltransferase, DmHen1, modifies germline piRNAs and single-stranded siRNAs in RISC. Curr Biol. 2007; 17: 1265–1272. https://doi.org/10.1016/j.cub.2007.06.030 PMID: 17604629

22. Saito K, Sakaguchi Y, Suzuki T, Suzuki T, Siomi H, Siomi MC. Pimet, the Drosophila homolog of HEN1, mediates 2′-O-methylation of Piwi- interacting RNAs at their 3′ ends. Genes Dev. 2007; 21: 1603–1608. https://doi.org/10.1101/gad.1563607 PMID: 17606638

23. Chan CM, Zhou C, Brunzelle JS, Huang RH. Structural and biochemical insights into 2′-O-methylation at the 3′-terminal nucleotide of RNA by Hen1. PNAS. 2009; 106: 17699–17704. https://doi.org/10.1073/pnas.0907540106 PMID: 19822745

24. Peng L, Zhang F, Shang R, Wang X, Chen J, Chou JJ, et al. Identification of substrates of the small RNA methyltransferase Hen1 in mouse spermatogonial stem cells and analysis of its methyl-transfer domain. J Biol Chem. 2018; 293: 9981–9994. https://doi.org/10.1074/jbc.RA117.000837 PMID: 29703750

25. Kirino Y, Mourelatos Z. The mouse homolog of HEN1 is a potential methylase for Piwi-interacting RNAs. RNA. 2007; 13: 1397–1401. https://doi.org/10.1261/rna.659307 PMID: 17652135

26. Kamminga LM, Luteijn MJ, den Broeder MJ, Redl S, Kaaij LJT, Roovers EF, et al. Hen1 is required for oocyte development and piRNA stability in zebrafish. EMBO J. 2010; 29: 3688–3700. https://doi.org/10.1038/emboj.2010.233 PMID: 20859253

27. Huang RH. Unique 2′-O-Methylation by Hen1 in Eukaryotic RNA Interference and Bacterial RNA Repair. Biochemistry. 2012; 51: 4087–4095. https://doi.org/10.1021/bi300497x PMID: 22564049

28. Zhao LN, Kaldis P. Cascading proton transfers are a hallmark of the catalytic mechanism of SAM-dependent methyltransferases. FEBS Letters. 2020; 594: 2128–2139. https://doi.org/10.1002/1873-3468.13799 PMID: 32353165

29. Fiser A, Do RK, Sali A. Modeling of loops in protein structures. Protein Sci. 2000; 9: 1753–1773. https://doi.org/10.1110/ps.9.9.1753 PMID: 11045621

30. Singh N, Warshel A. Absolute binding free energy calculations: On the accuracy of computational scoring of protein–ligand interactions. Proteins: Structure, Function, and Bioinformatics. 2010; 78: 1705–1723. https://doi.org/10.1002/prot.22687 PMID: 20186976

31. Sham YY, Chu ZT, Warshel A. Consistent Calculations of pKa's of Ionizable Residues in Proteins: Semi-microscopic and Microscopic Approaches. J Phys Chem B. 1997; 101: 4458–4472. https://doi.org/10.1021/jp963412w

32. King G, Warshel A. A surface constrained all-atom solvent model for effective simulations of polar solutions. J Chem Phys. 1989; 91: 3647–3661. https://doi.org/10.1063/1.456845

33. Yoon H, Zhao LN, Warshel A. Exploring the Catalytic Mechanism of Cas9 Using Information Inferred from Endonuclease VII. ACS Catal. 2019; 9: 1329–1336. https://doi.org/10.1021/acscatal.8b04324 PMID: 34046245

34. Zhao LN, Mondal D, Warshel A. Exploring alternative catalytic mechanisms of the Cas9 HNH domain. Proteins: Structure, Function, and Bioinformatics. 2020; 88: 260–264. https://doi.org/10.1002/prot.25796 PMID: 31390092
35. Lee FS, Chu ZT, Warshel A. Microscopic and semimicroscopic calculations of electrostatic energies in proteins by the POLARIS and ENZYMIX programs. Journal of Computational Chemistry. 1993; 14: 161–185. https://doi.org/10.1002/jcc.540140205
36. Frisch MJ, Trucks GW, Schlegel HB, Scuseria GE, Robb MA, Cheeseman JR, et al. Gaussian˜16 Revision C.01. 2016.
37. Thaplyal P, Bevilacqua PC. Experimental Approaches for Measuring pKa's in RNA and DNA. Methods Enzymol. 2014; 549: 189–219. https://doi.org/10.1016/B978-0-12-801122-5.00009-X PMID: 25432750
38. Li H, Robertson AD, Jensen JH. Very fast empirical prediction and rationalization of protein pKa values. Proteins. 2005; 61: 704–721. https://doi.org/10.1002/prot.20660 PMID: 16231289
39. Mordasini T, Curioni A, Andreoni W. Why Do Divalent Metal Ions Either Promote or Inhibit Enzymatic Reactions? Journal of Biological Chemistry. 2003; 278: 4381–4384. https://doi.org/10.1074/jbc.C200664200 PMID: 12496295
40. Ayadi L, Galvanin A, Pichot F, Marchand V, Motorin Y. RNA ribose methylation (2′-O-methylation): Occurrence, biosynthesis and biological functions. Biochimica et Biophysica Acta (BBA)—Gene Regulatory Mechanisms. 2019; 1862: 253–269. https://doi.org/10.1016/j.bbagrm.2018.11.009 PMID: 30572123
41. Bock CW, Katz AK, Markham GD, Glusker JP. Manganese as a Replacement for Magnesium and Zinc: Functional Comparison of the Divalent Ions. J Am Chem Soc. 1999; 121: 7360–7372. https://doi.org/10.1021/ja9906960
42. Kretsinger RH. Magnesium in Biological Systems. In: Kretsinger RH, Uversky VN, Permyakov EA, editors. Encyclopedia of Metalloproteins. New York, NY: Springer; 2013. pp. 1250–1255. https://doi.org/10.1007/978-1-4614-1533-6_258
43. Tang S, Yang JJ. Magnesium Binding Sites in Proteins. In: Kretsinger RH, Uversky VN, Permyakov EA, editors. Encyclopedia of Metalloproteins. New York, NY: Springer; 2013. pp. 1243–1250. https://doi.org/10.1007/978-1-4614-1533-6_257
44. Zheng H, Cooper DR, Porebski PJ, Shabalin IG, Handing KB, Minor W. CheckMyMetal: a macromolecular metal-binding validation tool. Acta Crystallogr D Struct Biol. 2017; 73: 223–233. https://doi.org/10.1107/S2059798317001061 PMID: 28291757
45. Zheng H, Chordia MD, Cooper DR, Chruszcz M, Müller P, Sheldrick GM, et al. Validation of metal-binding sites in macromolecular structures with the CheckMyMetal web server. Nat Protoc. 2014; 9: 156–170. https://doi.org/10.1038/nprot.2013.172 PMID: 24356774
46. Jain R, Shuman S. Bacterial Hen1 is a 3′ terminal RNA ribose 2′-O-methyltransferase component of a bacterial RNA repair cassette. RNA. 2010; 16: 316–323. https://doi.org/10.1261/rna.1926510 PMID: 20007328
47. Maguire ME, Cowan JA. Magnesium chemistry and biochemistry. Biometals. 2002; 15: 203–210. https://doi.org/10.1023/a:1016058229972 PMID: 12206387
48. Diebler H, Eigen M, Ilgenfritz G, Maass G, Winkler R. Kinetics and mechanism of reactions of main group metal ions with biological carriers. Pure and Applied Chemistry. 1969; 20: 93–116. https://doi.org/10.1351/pac196920010093
49. Vilkaitis G, Plotnikova A, Klimasauskas S. Kinetic and functional analysis of the small RNA methyltransferase HEN1: The catalytic domain is essential for preferential modification of duplex RNA. RNA. 2010; 16: 1935–1942. https://doi.org/10.1261/rna.2281410 PMID: 20705645
50. Yao J, Xie M, Ma X, Song J, Wang Y, Xue X. PIWI-interacting RNAs in cancer: Biogenesis, function, and clinical significance. Frontiers in Oncology. 2022; 12. Available: https://www.frontiersin.org/articles/10.3389/fonc.2022.965684 PMID: 36212439